

# Paramagnetic relaxation enhancement to improve sensitivity of fast NMR methods: application to intrinsically disordered proteins

François-Xavier Theillet · Andres Binolfi ·  
Stamatis Liokatis · Silvia Verzini · Philipp Selenko

Received: 29 July 2011 / Accepted: 28 September 2011 / Published online: 19 October 2011  
© Springer Science+Business Media B.V. 2011

**Abstract** We report enhanced sensitivity NMR measurements of intrinsically disordered proteins in the presence of paramagnetic relaxation enhancement (PRE) agents such as Ni<sup>2+</sup>-chelated DO2A. In proton-detected <sup>1</sup>H-<sup>15</sup>N SOFAST-HMQC and carbon-detected (H-flip)<sup>13</sup>CO-<sup>15</sup>N experiments, faster longitudinal relaxation enables the usage of even shorter interscan delays. This results in higher NMR signal intensities per units of experimental time, without adverse line broadening effects. At 40 mmol·L<sup>-1</sup> of the PRE agent, we obtain a 1.7- to 1.9-fold larger signal to noise (S/N) for the respective 2D NMR experiments. High solvent accessibility of intrinsically disordered protein (IDP) residues renders this class of proteins particularly amenable to the outlined approach.

**Keywords** Intrinsically disordered proteins · Alpha-synuclein · Histone H3 · Paramagnetic relaxation enhancement · Direct carbon detection · SOFAST-HMQC

## Introduction

Over the past years, a number of fast two-dimensional methods that exploit short longitudinal relaxation have been reported for proton and carbon-detected NMR

experiments (Felli and Brutscher 2009; Bermel et al. 2009; Schanda 2009; Farjon et al. 2009). These methods are especially well-suited for situations in which protein concentrations are limited, when fast, time-resolved NMR readouts are desired, or when unfavorable chemical exchange properties hamper NMR detection (Liokatis et al. 2010; Dose et al. 2011; Bertini et al. 2011; Ito and Selenko 2010). They collectively take advantage of selective excitation pulses and thereby ensure that a protein's relaxation behavior is governed by its longitudinal relaxation rate ( $1/T_1$ ), which is typically one order of magnitude larger than that of water. Faster recovery of equilibrium magnetization permits shorter recycling delays and conversely faster sampling rates, which give rise to higher NMR signal intensities per unit of experimental time.

Following this rationale, we reasoned that compounds that further enhanced protein  $T_1$  relaxation should offer the possibility of even greater time-savings, by permitting yet shorter recycling delays, thereby enabling NMR recordings of higher sensitivity in the same amount of experimental time. Here, transition metals that induce paramagnetic relaxation enhancement (PRE) have been shown to be particularly useful. 'Signal-enhancing' PRE effects have been exploited in solid (Wickramasinghe et al. 2009; Linser et al. 2007; Nadaud et al. 2009; Yamamoto et al. 2010), and solution-state NMR studies (Cai et al. 2006; Eletsky et al. 2003; Takeuchi et al. 2010a, b, c; Hiller et al. 2005; Otting and Liepinsh 1995). Could metal PREs also prove useful in fast longitudinal relaxation-optimized NMR experiments that already exhibit protein  $T_1$  times of less than half a second? PRE compounds that contain chelated Gd<sup>3+</sup> or Mn<sup>2+</sup>, at concentrations of ~5 mM have been shown to yield  $T_1$  times in that range, but higher amounts of these agents induce severe line broadening due to concomitant increases in transverse relaxation rates

**Electronic supplementary material** The online version of this article (doi:10.1007/s10858-011-9577-2) contains supplementary material, which is available to authorized users.

F.-X. Theillet · A. Binolfi · S. Liokatis · S. Verzini ·  
P. Selenko (✉)

Department of NMR-assisted Structural Biology, In-cell NMR  
Group, Leibniz Institute of Molecular Pharmacology (FMP),  
Robert-Roessle Str. 10, 13125 Berlin, Germany  
e-mail: selenko@fmp-berlin.de

(Cai et al. 2006; Eletsky et al. 2003; Hiller et al. 2005). Chelated  $\text{Ni}^{2+}$ , or  $\text{Co}^{2+}$  were thought to be better suited for the desired effect i.e. to further decrease  $T_1$  without affecting  $T_2$ , because of their electronic relaxation times in the range of  $T_c \sim 10^{-10}$  s (Bertini et al. 1996; Cai et al. 2006), which is much shorter than the average correlation times ( $T_c$ ) of proteins. When  $\text{Ni}^{2+}$ , or  $\text{Co}^{2+}$  are prevented from direct interactions with the proteins under investigation by ‘chelating’ them in inert organic compound cages for example, it should be possible to productively exploit paramagnetic relaxation enhancements in combination with fast NMR methods. Furthermore, we reasoned that in order for the envisaged PRE effect to enhance protein NMR signals in a uniform manner, most protein residues were to be solvent exposed and PRE compound accessible. Clearly, this is not the case in folded proteins, or folded protein domains. Therefore, intrinsically disordered proteins (IDPs), proteins that lack secondary/tertiary structure and a buried hydrophobic core (Uversky et al. 2008), were deemed ideal targets for the outlined approach.

In the following, we report 2D  $^1\text{H}$ - $^{15}\text{N}$  SOFAST-HMQC and 2D (H-flip) $^{13}\text{C}$ - $^{15}\text{N}$  NMR experiments (Schanda et al. 2005; Bermel et al. 2009) in the presence of  $\text{Ni}^{2+}$  coordinated 1,4,7,10-Tetraazacyclododecane-1,7-bis(acetate) ( $\text{DO2A}^{2-}$ ). Human alpha synuclein (AS), a 140-residue model IDP, and the disordered first 33 residues of histone H3 (H3 aa 1-33) function as target proteins. DO2A was chosen because of its ability to bind transition metals at subfemtomolar affinity (Chang et al. 1999) and because the resulting metal-DO2A complexes are charge neutral (Suppl. Fig. 1). Our results demonstrate that the use of Ni-DO2A accelerated protein  $T_1$  relaxation in the above NMR experiments, which produced higher NMR signal intensities per units of experimental time. In the presence of 40 mM Ni-DO2A NMR signals were enhanced  $\sim 2.5$ -fold in 1D  $^1\text{H}$ - $^{15}\text{N}$  SOFAST-HMQC experiments, and  $\sim 1.9$ -fold in 1D (H-flip) $^{13}\text{C}$ - $^{15}\text{N}$  experiments at 750 MHz (17.6 T). Signal enhancements in the respective 2D NMR experiments were  $\sim 1.9$ -fold for the  $^1\text{H}$ - $^{15}\text{N}$  SOFAST-HMQC sequence and  $\sim 1.7$ -fold for the (H-flip) $^{13}\text{C}$ - $^{15}\text{N}$  pulse program.

## Materials and methods

### Isotope labeled protein production

Histone H3 (aa1-33) was recombinantly produced as previously described (Liokatis et al. 2010). Human wild-type AS was expressed from a pT7-7 plasmid in *E. coli* BL21 (DE3) Express after overnight induction (1 mM IPTG) at 303 K and an  $\text{OD}_{600}$  of 0.6. The recombinant protein was purified to homogeneity following the protocol by Hoyer et al. (2002).

### Ni-DO2A production

DO2A (1,4,7,10-Tetraazacyclododecane-1,7-bis(acetic acid)) was purchased from Chematech (Dijon, France) in the form of a lyophilized powder (DO2A, 2HCl). Nickel(II)-sulfate-hexahydrate was purchased from Roth GmbH, Cobalt(II)-chlorid-hexahydrate from Applichem. PRE complexes were obtained by mixing stoichiometric amounts of DO2A and metal-ions at concentrations of about  $1 \text{ mol}\cdot\text{L}^{-1}$ . Addition of NaOH was necessary to achieve a neutral pH, which coincided with a color change from blue to purple for  $\text{Ni}^{2+}$  and from purple to red for  $\text{Co}^{2+}$ . Salt ( $\text{Na}^+$ ,  $\text{Cl}^-$ ,  $\text{SO}_4^{2-}$ ) and excess metal removal was achieved via a Dowex Retardion 11A8 ion-exchange column, purchased from Sigma-Aldrich. Two to three passages, each of them followed by a lyophilization- and dissolving step were employed to yield Ni-DO2A concentrations between 0.5 and  $1 \text{ mol}\cdot\text{L}^{-1}$ . The final concentration of the metal-ion DO2A stock solution was adjusted to  $0.5 \text{ mol}\cdot\text{L}^{-1}$ .

### NMR spectroscopy

All NMR spectra were recorded with 3 mm diameter Shigemi tubes, on a 750 MHz Bruker Avance spectrometer, equipped with a cryogenically cooled triple resonance  $^1\text{H}\{^{13}\text{C}/^{15}\text{N}\}$  TCI probe. For all quantitative analyses-, in order to ensure optimal S/N and to enable fast NMR measurements of the individual data points-, NMR experiments were carried out at protein concentrations of 250  $\mu\text{M}$  for AS, or at 1 mM for H3. AS was measured in 40 mM sodium phosphate, 150 mM NaCl buffer at pH 6.4. H3 was measured in 40 mM sodium phosphate, 150 mM NaCl buffer at pH 6.8. Ni-DO2A was added to final concentrations of 10, 20, and 40 mM. All sample volumes were 150  $\mu\text{L}$ . pH changes were checked after every experiment and found to be less than 0.02 pH units. 1D and 2D  $^1\text{H}$ - $^{15}\text{N}$  SOFAST-HMQC experiments (Schanda et al. 2005) were recorded at 283 and 303 K. 1D NMR spectra were recorded with 128 scans and the indicated interscan delays. 2D NMR spectra were performed with 16 scans, 1,024 complex points for a sweep width of 16.6 ppm for the  $^1\text{H}$  dimension (zero-filling to 4,096 points), with 512 complex points for the  $^{15}\text{N}$  dimension ( $t_1$ ) and a sweep width of 28 ppm (zero-filling to 1,024 points), and an acquisition time of 42 ms, using an interscan delay of 30 ms. A proton  $90^\circ$  polychromatic PC9 pulse of 2,400  $\mu\text{s}$  and a REBURP  $180^\circ$  pulse of 1,600  $\mu\text{s}$  were employed. A refocusing carbon pulse was used in the middle of the HMQC scheme.  $^{15}\text{N}$ -decoupling during the acquisition period was achieved with the Waltz-16 sequence at 1.25 kHz (Shaka et al. 1983).  $^{13}\text{C}$ - $^{15}\text{N}$  (H-flip)CON experiments (Bermel et al. 2009) were recorded at 283 and 303 K, with 512 scans and the indicated interscan delays

for 1D NMR spectra. 2D NMR experiments were recorded with 64 scans, 1,024 complex points and a sweep width of 32 ppm for the direct  $^{13}\text{C}$  dimension. 128 increments (resulting from 256 IPAP increments) and a sweep width of 28 ppm for the  $^{15}\text{N}$  dimension, an acquisition time of 82 ms and an interscan delay of 130 ms were used. Q5 and Q3 gaussian cascades (Emsley and Bodenhausen 1992) were employed for the  $^{13}\text{C}$  pulses;  $90^\circ$  Q5 pulses of 860  $\mu\text{s}$  for  $\text{C}\alpha$  and of 274  $\mu\text{s}$  for alkyl or carbonyl carbons, and  $180^\circ$  Q3 pulses of 220  $\mu\text{s}$  for alkyl or carbonyl carbons.  $\text{C}\alpha$  and alkyl selective pulses were centered at 52 ppm, CO selective pulses were centered at 176 ppm.

To obtain residue-resolved enhancement plots ( $I/I_0$ ), amide envelope integrals of the 1D NMR spectra, and peak heights of non-overlapped 2D NMR signals in  $^1\text{H}$ - $^{15}\text{N}$  SOFAST-HMQC and (H-flip) $^{13}\text{C}$ - $^{15}\text{N}$  experiments were compared in the absence ( $I_0$ ) and presence ( $I$ ) of Ni-DO2A. All data were processed and analyzed in Topspin 2 (Bruker) and iNMR 3.6.3. 2D NMR spectra were analyzed in Sparky (Goddard and Kneller, UCSF). Curves were fitted and plotted using GraphPad Prism 5.0.

## Results

### Ni-DO2A PRE effects in 1D NMR experiments

To test the overall feasibility of the presented approach, we performed initial one-dimensional (1D)  $^1\text{H}$ - $^{15}\text{N}$  SOFAST-HMQC experiments on either  $^{15}\text{N}$ - $^{13}\text{C}$ -, or  $^{15}\text{N}$ -labeled recombinant AS in the presence of increasing amounts (10–40 mM) of Ni-DO2A. All of the experimentally obtained results were identical for the two differently labeled versions of the protein. Overall NMR signal intensities were calculated by integration of the complete ‘amide envelope’ of the corresponding 1D traces at different recycling delays. Signal intensities were measured at 283 and 303 K (pH 6.4) to sample different proton exchange regimes, as well as to assess temperature-dependent changes in the protein’s correlation time. Recovery of equilibrium magnetization

was progressively accelerated with increasing amounts of the PRE compound at both 283 and 303 K. We delineated an apparent recovery time ( $T_1^*$  in seconds, Table 1) that was fitted to the respective buildup curves (Fig. 1a), using the following equation:

$$I(t_{\text{scan}}) = I_0 * \left( 1 - \exp\left(-\frac{t_{\text{scan}} - t_{\text{rf}}}{T_1^*}\right) \right) \quad (1)$$

with

$$t_{\text{scan}} - t_{\text{rf}} = t_{\text{acq}} + t_{\text{delay}} = t_{\text{rec}} \quad (2)$$

where  $t_{\text{scan}}$  denotes the total length of one scan,  $t_{\text{rf}}$  is the length of the pulse sequence,  $t_{\text{rec}}$  is the magnetization recovery time between consecutive pulse trains,  $t_{\text{acq}}$  is the acquisition period and  $t_{\text{delay}}$  is the delay between individual scans. For the  $^1\text{H}$ - $^{15}\text{N}$  SOFAST-HMQC pulse sequence,  $T_1^*$  of AS in the presence of increasing amounts of Ni-DO2A approximated a  $T_{1^*_{\text{min}}}$  value (shortest  $T_1^*$ ) of  $\sim 70$  ms. Overall, enhanced spin–lattice relaxation increased the efficiency of the  $^1\text{H}$ - $^{15}\text{N}$  SOFAST-HMQC pulse sequence in terms of sensitivity, when defined as the total signal intensity per unit of experimental time (Fig. 1b). At 40 mM Ni-DO2A, overall sensitivity was enhanced 2.5-fold (283 K) or 1.8-fold (303 K), when compared to the reference NMR experiment in the absence of the PRE compound (set to 1). At Ni-DO2A concentrations above 40 mM, no further signal enhancements were detected. In fact, greater  $T_2$  relaxation resulted in an overall reduction of NMR signal intensities (Suppl. Fig. 2).

$T_1^*$  was shorter at 303 K than at 283 K, which was likely caused by the different amide proton/water chemical exchange regimes at these temperatures. Indeed, water magnetization is maintained along  $+z$  during the  $^1\text{H}$ - $^{15}\text{N}$  SOFAST-HMQC experiment (Suppl. Fig. 3). This residual water magnetization is employed as an effective magnetization reservoir for those amide protons that readily exchange with water during the recovery time. Thus, the initial magnetization that is available for any given amide proton population at the beginning of each scan  $M_z^{b,\text{eq}}$  is given by:

**Table 1**  $T_1^*$  (in seconds) from fitting of progress curves  $I(t_{\text{scan}})$

[Ni-DO2A] (mmol·L <sup>-1</sup> )	$^1\text{H}$ - $^{15}\text{N}$ SOFAST-HMQC				(H-flip) $^{13}\text{C}$ - $^{15}\text{N}$			
	AS		H3 aa1-33		AS		H3 aa1-33	
	283 K	303 K	283 K	303 K	283 K	303 K	283 K	303 K
0	0.28	0.15	0.14	0.07	0.22	0.24	0.20	0.21
10	0.17	0.10	0.09	0.04	0.14	0.15	0.13	0.13
20	0.13	0.08	0.07	0.03	0.10	0.11	0.09	0.10
40	0.09	0.07	0.06	0.03	0.08	0.09	0.07	0.08

Errors were calculated from two independent experiments after curve fitting. The average error is  $\sim 10\%$  for every  $T_1^*$

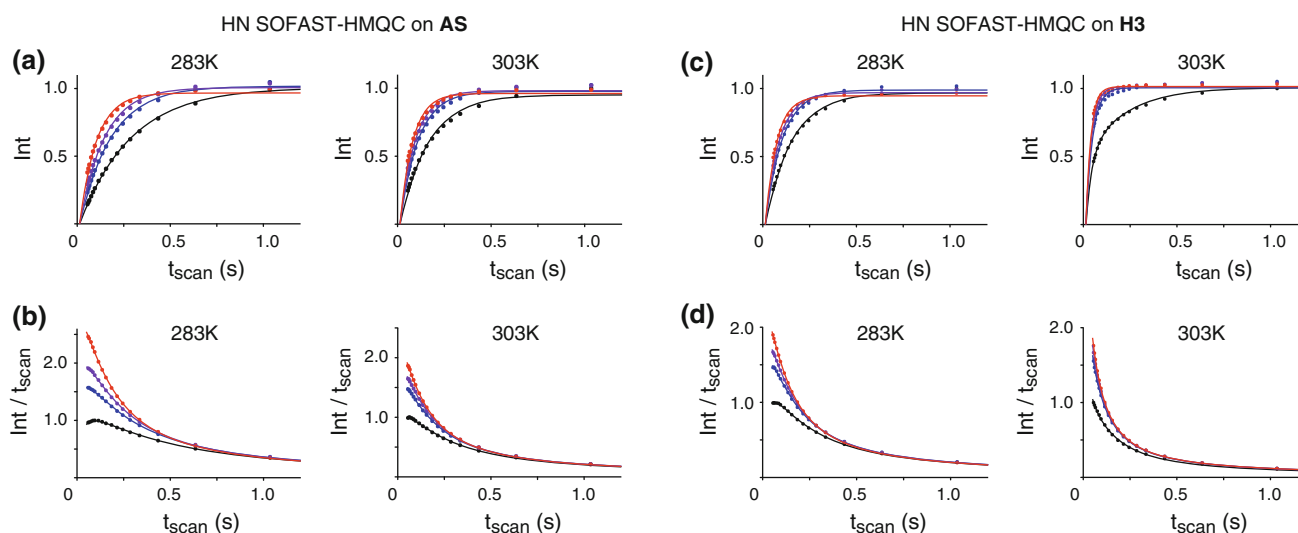


**Fig. 1** Ni-DO2A mediated signal enhancements in proton-detected 1D NMR experiments. Curves on top represent absolute signal intensities determined from 1D  $^1\text{H}$ - $^{15}\text{N}$  SOFAST-HMQC experiments on (a) alpha-synuclein (AS) or (c) histone H3. The integral of the complete ‘amide envelope’ is plotted as a function of scan time ( $t_{\text{scan}}$ ). Ni-DO2A concentrations were 0 mM (black), 10 mM (blue), 20 mM (purple) and 40 mM (red). Data for 283 and 303 K are shown.

$$M_z^{b,\text{eq}} \propto M_0 * \left( 1 - \exp \left[ -t_{\text{rec}} * \left( \frac{1}{T_{1,\text{selectHN}}} + \frac{1}{T_{\text{ex,wat-HN}}} \right) \right] \right) \quad (3)$$

where  $M_0$  is the thermal equilibrium magnetization,  $T_{1,\text{selectHN}}$  is the longitudinal relaxation time of the residue-specific amide proton in the  $^1\text{H}$ - $^{15}\text{N}$  SOFAST-HMQC experiment, and  $T_{\text{ex,wat-HN}}$  is the characteristic water/amide proton chemical exchange time. Clearly,  $T_{\text{ex,wat-HN}}$  is different for different protein residues, which makes it difficult to achieve a satisfying global fit with 1D spectra only. The important point to stress is that low  $T_{\text{ex,wat-HN}}$ , due to high temperature or high pH, reduces the benefit of Ni-DO2A on  $T_1^*$ , even if its’ effect on  $T_{1,\text{selectHN}}$  is rather constant.

Equation (3) is similar to relations reported by Schanda (2009), for a flip angle of  $90^\circ$  that we employed in our experiments. For IDPs, the use of different Ernst angles was found to be of little advantage even at short  $t_{\text{scan}}$  times. As a matter of fact, flip angles other than  $90^\circ$  resulted in an overall loss of sensitivity at  $t_{\text{scan}}$  times greater than 70 ms at 303 K (Suppl. Fig. 4).

Separation of  $T_1^*$  into purely longitudinal relaxation and water-amide exchange-terms was more straightforward in case of the second protein that we employed in our study, the N-terminus of histone H3. At 303 K and at pH 6.8, prominent chemical exchange behavior of many peptide residues dominated the spin–lattice relaxation rate. Therefore, NMR signal enhancements at increasing concentrations of Ni-DO2A were less pronounced than for AS (Fig. 1c). At

Bottom curves (b) and (d) display the same data as ‘NMR signal intensities per unit of experimental time ( $\text{Int}/t_{\text{scan}}$ )’ against the total scan time. The highest measured signal intensity in the absence of PRE compound was set to 1. All other signal intensities were determined with respect to this normalized intensity. Each curve was fitted to (1), except for H3 at 0 mM Ni-DO2A and 303 K, for which two  $T_1^*$  values were employed

40 mM of Ni-DO2A, 1.9-fold (283 K) and 1.8-fold (303 K) enhancements were obtained (Fig. 1d). In analogy to AS, these numbers were smaller at higher temperatures. In summary, addition of Ni-DO2A (40 mM) to different IDP samples enabled sensitivity increases up to 2.5-fold in  $^1\text{H}$ - $^{15}\text{N}$  SOFAST-HMQC experiments. For proteins that exhibited fast amide proton/water exchange behaviors, the obtained signal enhancements were generally lower.

Next, we extended our analyses to (H-flip) $^{13}\text{CO}$ - $^{15}\text{N}$  carbon-detected NMR experiments. Only non-exchangeable nuclei ( $\text{H}\alpha$ ,  $\text{C}\alpha$ , CO, N) are manipulated in this pulse sequence so that no chemical exchange effects are encountered. Similar NMR signal enhancements with increasing amounts of Ni-DO2A were experimentally determined at different temperatures (Fig. 2a, b). For the (H-flip) $^{13}\text{CO}$ - $^{15}\text{N}$  pulse sequence,  $T_1^*$  of AS, at 40 mM of Ni-DO2A resulted in a  $T_{1,\text{min}}^*$  of  $\sim 70$  ms. Maximum signal intensities were reached at a  $t_{\text{scan}}$  time of about 250 ms (Fig. 2b). Overall, sensitivity was enhanced  $\sim 1.9$ -fold at both 283 and 303 K. Similar results were obtained for the H3 peptide (Fig. 2c, d), which confirmed that the observed Ni-DO2A effects were rather independent of IDP size and flexibility.

#### Ni-DO2A PRE effects in 2D NMR experiments

Our main objective was to obtain similar signal enhancements in two-dimensional (2D) versions of the above NMR experiments. Initially, we recorded 2D  $^1\text{H}$ - $^{15}\text{N}$  SOFAST-HMQC spectra of AS at 283 and 303 K, with average  $t_{\text{scan}}$

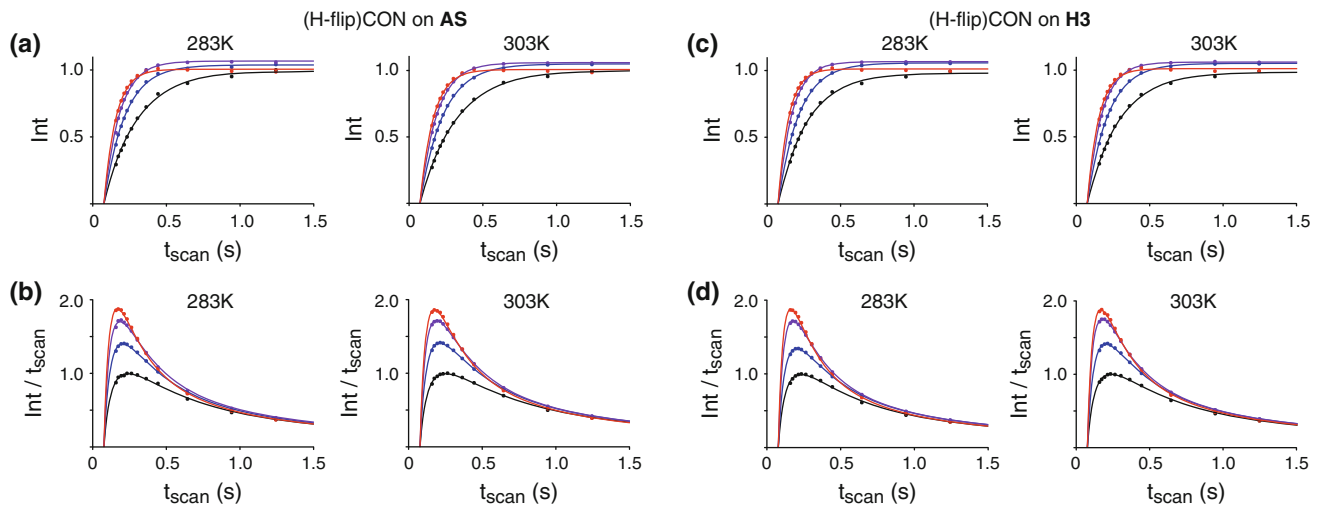


**Fig. 2** Ni-DO2A mediated signal enhancements in carbon-detected 1D NMR experiments. Curves on top represent absolute signal intensities determined from 1D (H-flip) $^{13}\text{C}/^{15}\text{N}$  experiments on (a) AS or (c) histone H3. The integral of the complete  $^{\circ}$ carbonyl envelope $^{\circ}$  is plotted as a function of scan time ( $t_{\text{scan}}$ ). Ni-DO2A concentrations were 0 mM (black), 10 mM (blue), 20 mM (purple)

and 40 mM (red). Data for 283 and 303 K are shown. Bottom curves (b) and (d) display the same data as ‘NMR signal intensities per unit of experimental time ( $\text{Int}/t_{\text{scan}}$ )’ against the total scan time. The highest measured signal intensity in the absence of PRE compound was set to 1. All other signal intensities were determined with respect to this normalized intensity

times of 115 ms. A fully resolved 2D NMR spectrum of AS, at 40 mM of Ni-DO2A, revealed uniform signal enhancements that ranged from 1.5- to 2.3-fold at 283 K (Fig. 3a). Average signal intensities were 1.9-fold larger and average AS linewidths in the proton dimension increased from 34 to 38 Hz (40 mM Ni-DO2A) at 283 K. At 303 K, NMR signal intensities were 1.45-fold larger (Fig. 3b). In the presence of 40 mM Ni-DO2A, NMR linewidths in the proton dimension increased from 38 to 39 Hz (Fig. 3), while they increased from 6.5 to 8 Hz, on average, in the indirect  $^{15}\text{N}$  dimension (data not shown). Thus, overall spectral resolution was only slightly affected by the presence of the PRE agent (Figs. 3, 4a).

Next, we recorded  $^{13}\text{C}$ -detected 2D (H-flip) $^{13}\text{C}/^{15}\text{N}$  experiments on AS at 303 K with an average  $t_{\text{scan}}$  of 330 ms (Fig. 3c). Residue specific enhancements in the presence of 40 mM of Ni-DO2A were 1.3- to 2.0-fold for this experiment, with an average enhancement factor of 1.7. In the  $^{13}\text{C}$ -detected NMR experiments, the carbon linewidths ( $\sim 18$  Hz) were insensitive to the presence of the PRE agent (Figs. 3c, 4b).

Higher NMR signal intensities in the presence of Ni-DO2A may alternatively be used to record more points in indirect dimensions within in the same amount of experimental time, i.e. to increase spectral resolution. As an example, we measured 2D  $^1\text{H}/^{15}\text{N}$  SOFAST-HMQC experiments of AS in the absence of PRE agent with 64 scans and 176 complex points in the indirect dimension (digital resolution  $\sim 12$  Hz, zero filling to 1 Hz, Fig. 5a) and in the presence of 40 mM Ni-DO2A with 16 scans and

512 complex points (digital resolution  $\sim 4$  Hz, zero filling to 1 Hz, Fig. 5b). Both experiments required the same amounts of experimental time and yielded identical signal to noise ratios. However, the presence of the PRE agent enabled recordings of much higher spectral resolution. Similar results were obtained for the H3 sample. At 40 mM Ni-DO2A, average signal enhancements were 1.3-fold at both temperatures for the  $^1\text{H}/^{15}\text{N}$  SOFAST-HMQC experiments, and 1.7-fold for the (H-flip) $^{13}\text{C}/^{15}\text{N}$  experiment (Suppl. Fig. 5).

To investigate whether certain amino acids of AS responded differently to the employed PRE agent, we sorted the observed enhancements by residue type (Suppl. Fig. 6). Protein amino acids were divided into two groups according to their NH-water exchange properties (i.e. fast and slow). This classification was based on ‘primary’ amide exchange behaviors of amino acids in random coil conformations (Bai et al. 1993). At higher temperatures-, and employing the  $^1\text{H}/^{15}\text{N}$  SOFAST-HMQC pulse sequence-, these two classes of amino acids were clearly distinguishable. Residues with low  $T_{\text{ex,wat-HN}}$  benefited less from shorter  $T_{1,\text{selectHN}}$ . At 283 K, i.e. in a slower NH-water exchange time regime, no amino acid displayed pronounced deviations from the observed effect. This was also the case for all temperatures of the (H-flip) $^{13}\text{C}/^{15}\text{N}$  experiments, for which only non-exchangeable proton magnetization is used. These results are consistent with the notion that IDPs generally display homogeneous solvent accessibilities of most of their residues.

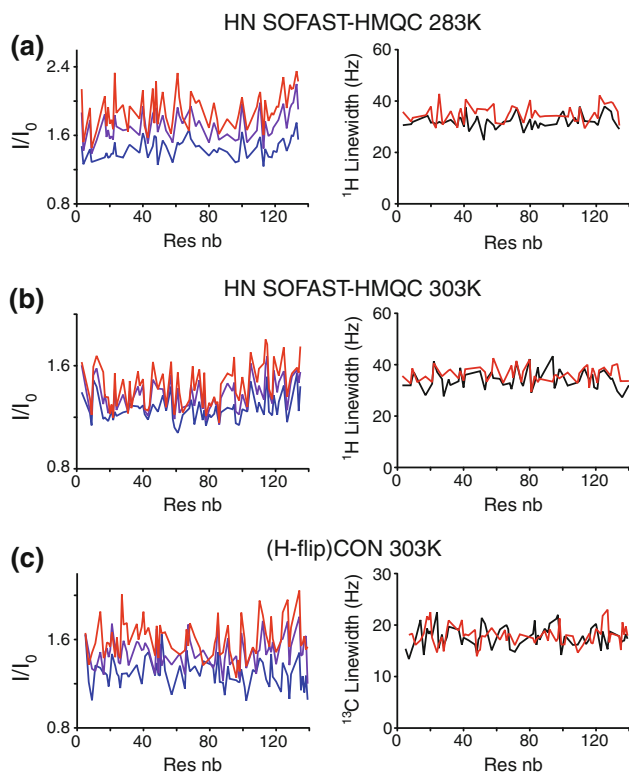


**Fig. 3** Residue-resolved enhancement analysis for proton- and carbon-detected 2D NMR experiments. NMR signal enhancements in 2D  $^1\text{H}$ - $^{15}\text{N}$  SOFAST-HMQC NMR experiments on AS at 283 K (a) and 303 K (b) as determined by resonance cross-peak intensity measurements are shown on the left. Ni-DO2A concentrations were 10 mM (blue), 20 mM (purple) and 40 mM (red). NMR signals in the absence of Ni-DO2A were set to 1. All other intensities were determined relative to this value. (c) NMR signal enhancements in 2D (H-flip) $^{13}\text{C}/^{15}\text{N}$  NMR experiments on AS at 303 K. Linewidths in the direct dimension ( $^1\text{H}$  for  $^1\text{H}$ - $^{15}\text{N}$  SOFAST-HMQC and  $^{13}\text{C}$  for (H-flip) $^{13}\text{C}$ - $^{15}\text{N}$ ) of well-separated cross-peaks at 0 mM (black) and 40 mM (red) Ni-DO2A were determined and are shown on the right. Two independent measurements produced an average error of less than 5%

In summary, addition of 40 mM Ni-DO2A to either a large, or a small IDP enabled enhanced sensitivity measurements of proton- and carbon-detected NMR experiments, without disadvantageous line-broadening effects, or chemical shift displacements (Fig. 4). With the outlined experimental setups, high resolution 2D  $^1\text{H}$ - $^{15}\text{N}$  SOFAST-HMQC and (H-flip) $^{13}\text{C}$ - $^{15}\text{N}$  NMR spectra of 80  $\mu\text{L}$  AS at 5  $\mu\text{M}$ , or at 125  $\mu\text{M}$ , respectively, were recorded in less than 1 hour (3 mm tube).

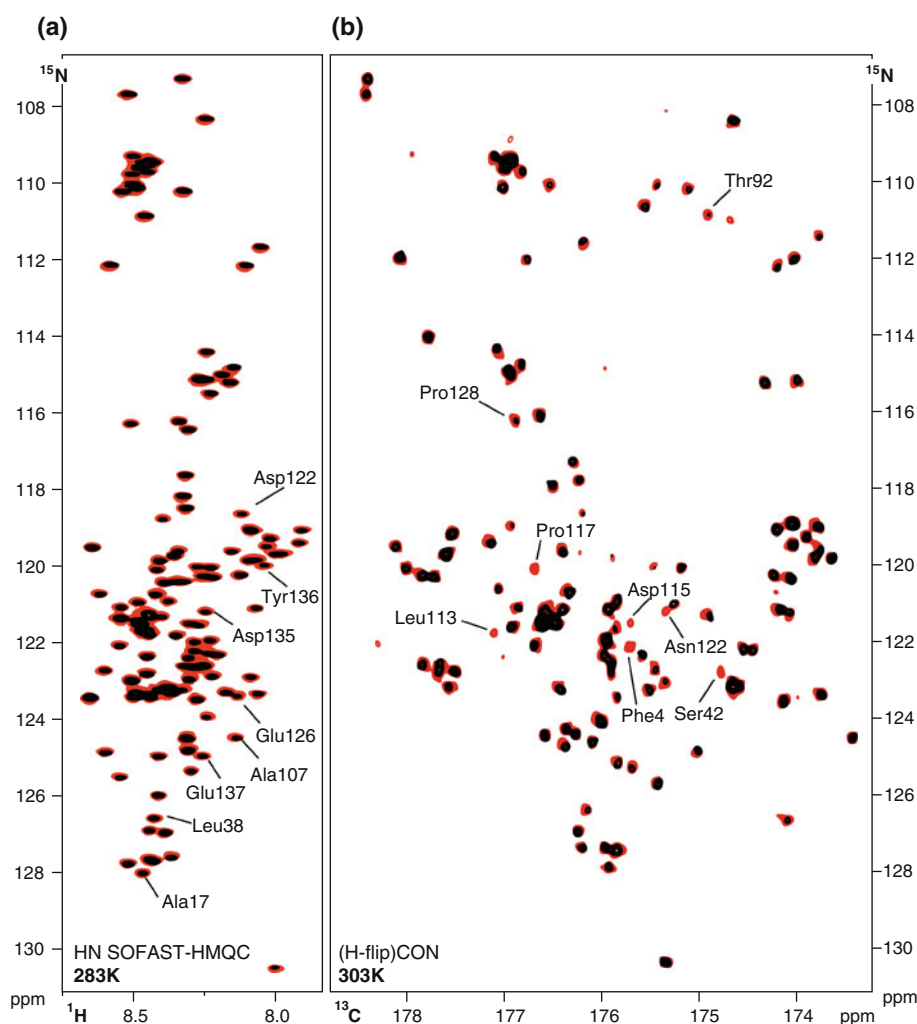
## Discussion

Potential benefits from chemical exchange-mediated water relaxation enhancements on protein amide signals have previously been reported for folded proteins (Hiller et al.

2005; Cai et al. 2006). Cai et al. rationalized that these PRE effects could lead to larger sensitivity enhancements in terminal-, or loop region residues, as compared to buried amino acids in the protein core. Here, we demonstrate that these considerations are valid for fast two-dimensional NMR methods and intrinsically disordered proteins. Different  $T_1$ 's at different pH settings and temperatures were obtained with  $^1\text{H}$ - $^{15}\text{N}$  SOFAST-HMQC sequences in the absence of the PRE compound. Water/amide proton exchange rates are accelerated at higher temperatures and higher pH, which allows faster amide magnetization recoveries because bulk solvent magnetization is 'stored' along  $+z$  during the pulse sequence. Fast exchanging amide protons recovered their longitudinal magnetization more rapidly than slow exchanging protons so that only the latter 'benefited' from longer interscan delays (Fig. 1c). This explains the low initial  $T_1^*$  value of the H3 peptide at higher temperature. Here, further enhancement of longitudinal relaxation by action of Ni-DO2A had less of an effect, because magnetization recovery was already very efficient. Similarly, Ni-DO2A-mediated sensitivity enhancement for AS decreases from 1.9-fold to 1.45-fold, on average, in the respective 2D NMR experiments at higher temperatures. No such dependencies were observed in the (H-flip) $^{13}\text{C}$ - $^{15}\text{N}$  experiments, because they do not manipulate exchangeable protons. Here, sensitivity enhancements were 1.7-fold for AS and 1.7-fold for H3, independent of temperature and pH. In fact, SOFAST-HMQC experiments were generally better suited for fast IDP NMR measurements than HSQC-type pulse sequences (Suppl. Fig. 7). This notion held true for settings in which Ni-DO2A was present, or absent.

A possible matter of concern is paramagnetic metal leakage from the DO2A cage and a concomitant 'direct' PRE effect on the measured proteins. In response, we argue that AS is especially well suited to rule out any such behavior because the protein is known to bind to different divalent metals (Rasia et al. 2005; Binolfi et al. 2006, 2008, 2011). Free  $\text{Ni}^{2+}$  ions in particular have AS dissociation constants in the range of 1 mM (Binolfi et al. 2006) and metal binding has been shown to result in characteristic chemical shift displacements, or in site-specific line broadening. None of these effects were observed in our NMR experiments, even at the highest PRE concentrations tested (i.e. 40 mM) (Fig. 4). To avoid trace amounts of free metals in the respective PRE agent, the 'metal-loaded' DO2A compound was purified twice over a metal retardation column and a third passage was employed immediately before the actual NMR experiments to exclude metal leakage due to compound aging during the storage process. We also performed analogous experiments with  $\text{Co}^{2+}$ -loaded DO2A and AS and obtained nearly identical NMR signal enhancement effects (data not shown). This agrees well with the comparable electron-spin relaxation

**Fig. 4** Signal enhancements in proton- and carbon-detected 2D NMR experiments. **(a)** Overlay of  $^1\text{H}$ - $^{15}\text{N}$  SOFAST-HMQC spectra of AS (283 K) at 0 mM (black) and 40 mM (red) Ni-DO2A, plotted at identical contour levels. NMR signal enhancements are readily visible. A random set of strongly enhanced residues is labeled. No chemical shift differences in the presence of Ni-DO2A are observed. **(b)** Overlay of (H-flip) $^{13}\text{C}$ - $^{15}\text{N}$  spectra of AS (303 K) at 0 mM (black) and 40 mM (red) Ni-DO2A, plotted at identical contour levels



times of both metals ( $10^{-11} - 10^{-13}$  s) (Bertini et al. 1996) and suggests that  $\text{Ni}^{2+}$  and  $\text{Co}^{2+}$  may be interchangeably used for the respective NMR experiments. In our hands, desalting of Co-DO2A species generated from  $\text{CoCl}_2 \cdot 6\text{H}_2\text{O}$  was less efficient than desalting Ni-DO2A obtained from  $\text{NiSO}_4 \cdot 6\text{H}_2\text{O}$ . Hence, we resorted to the preferred usage of Ni-DO2A for merely practical reasons.

In conclusion, the results presented here demonstrate that caged  $\text{Ni}^{2+}$  or  $\text{Co}^{2+}$  can be used for improved sensitivity measurements using fast NMR methods. Our experimental results suggest that IDPs might represent molecular targets that are particularly amenable to the outlined approach. The observed enhancements are expected to be of similar sizes-, or even slightly larger-, at higher magnetic field strengths, because of the modestly lower longitudinal relaxation rates, especially when selective amide proton excitation pulses are used (Schanda 2009). The usage of such PREs is particularly beneficial for time-resolved NMR studies of ‘fast’ reaction processes-, such as the establishment of post-translational protein

modifications, i.e. when low sample concentrations and quick readout schemes are required. Alternatively, this method may be employed in situations where protein amounts, or NMR measurement times are limited, or when higher spectral resolution in indirect dimensions is desired. At 17.6 T (750 MHz) and on a 5 mm cryogenically cooled TCI probe with 3 mm Shigemi sample tubes and in the presence of 30 mM Ni-DO2A, we routinely record ‘full’ 2D heteronuclear  $^1\text{H}$ - $^{15}\text{N}$  SOFAST-HMQC experiments at 5–10  $\mu\text{M}$  sample concentrations ( $\sim 1$  nmol in 100  $\mu\text{L}$ ) in less than 1 h. For  $^{13}\text{C}$ -detected 2D correlations using the (H-flip) $^{13}\text{C}$ - $^{15}\text{N}$  pulse sequence, 10 nmol of protein material (125  $\mu\text{M}$  in 80  $\mu\text{L}$ ) is sufficient to obtain similar results. On a cryogenically cooled probe that is optimized for direct  $^{13}\text{C}$  detection, a 3-times better overall signal to noise was achieved (Felli and Pierattelli, personal communication). In combination with the outlined PRE scheme, this may well push the limits of  $^{13}\text{C}$ -detected experiments into the low micromolar concentration range of biomolecular NMR measurements.

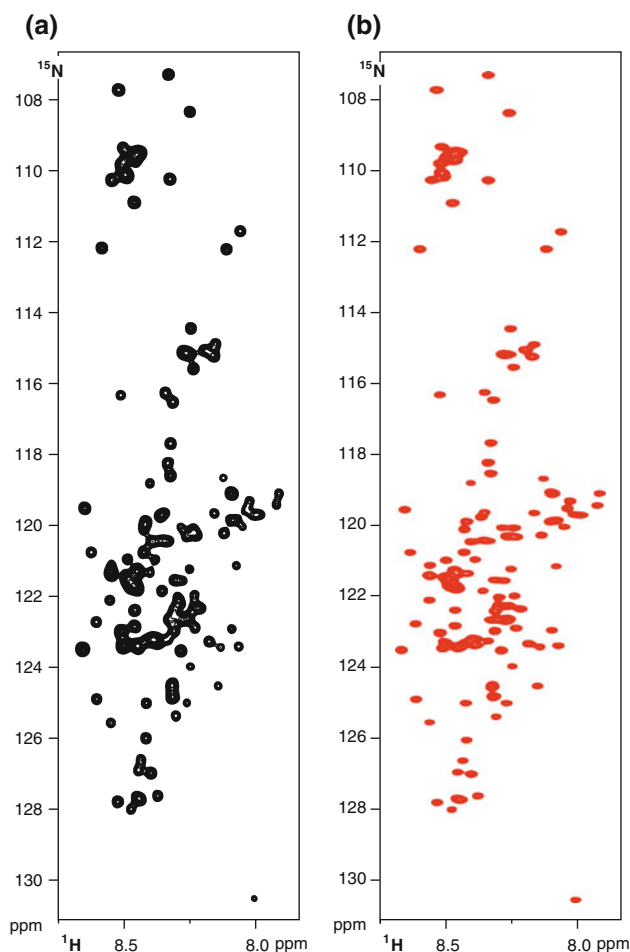


**Fig. 5** Exploiting PREs for higher resolution measurements. (a)  $^1\text{H}$ - $^{15}\text{N}$  SOFAST-HMQC spectra of AS (283 K) at 0 mM Ni-DO2A (black) with 64 scans and 176 complex points in the indirect dimension (digital resolution  $\sim 12$  Hz, zero filling to 1 Hz). The total experimental time was 19 min and 57 s. (b)  $^1\text{H}$ - $^{15}\text{N}$  SOFAST-HMQC spectra of AS (283 K) at 40 mM Ni-DO2A (red) with 16 scans and 512 complex points in the indirect dimension (digital resolution  $\sim 4$  Hz, zero filling to 1 Hz). The total experimental time was 20 min for both experiments, with interscan delays of 30 ms

**Acknowledgments** We thank Dr. Peter Schmieder and Monika Beerbaum for helpful discussions and excellent NMR infrastructure maintenance and Dr. Linda Ball for useful comments and carefully reading the manuscript. We additionally thank Dr. Roberta Pierattelli and Dr. Isabella Felli (CERM) for sharing information about benchmark TXO probe specifications using our samples. F.X.T was supported by a post-doctoral grant from the Association pour la Recherche contre le Cancer (ARC). P.S. is supported by an Emmy Noether program grant (SE-1794/1-1) by the Deutsche Forschungsgemeinschaft (DFG).

## References

- Bai Y, Milne JS, Mayne L, Englander SW (1993) Primary structure effects on peptide group hydrogen exchange. *Proteins* 17(1): 75–86
- Bermeil W, Bertini I, Felli IC, Pierattelli R (2009) Speeding Up C-13 direct detection biomolecular NMR spectroscopy. *J Am Chem Soc* 131(42):15339–15345
- Bertini I, Luchinat C, Aime S (1996) NMR of paramagnetic substances. *Coord Chem Rev* 150:1–292
- Bertini I, Felli IC, Gonnelli L, Kumar MVV, Pierattelli R (2011)  $^{13}\text{C}$  direct-detection biomolecular NMR spectroscopy in living cells. *Angew Chem Int Ed Engl* 50(10):2339–2341
- Binolfi A, Rasia RM, Bertocini CW, Ceolin M, Zweckstetter M, Griesinger C, Jovin TM, Fernandez CO (2006) Interaction of alpha-synuclein with divalent metal ions reveals key differences: a link between structure, binding specificity and fibrillation enhancement. *J Am Chem Soc* 128(30):9893–9901
- Binolfi A, Lamberto GR, Duran R, Quintanar L, Bertocini CW, Souza JM, Cervenansky C, Zweckstetter M, Griesinger C, Fernandez CO (2008) Site-specific interactions of Cu(II) with alpha and beta-synuclein: bridging the molecular gap between metal binding and aggregation. *J Am Chem Soc* 130(35): 11801–11812
- Binolfi A, Valiente-Gabioud AA, Duran R, Zweckstetter M, Griesinger C, Fernandez CO (2011) Exploring the structural details of Cu(I) binding to alpha-synuclein by NMR spectroscopy. *J Am Chem Soc* 133(2):194–196
- Cai S, Seu C, Kovacs Z, Sherry AD, Chen Y (2006) Sensitivity enhancement of multidimensional NMR experiments by paramagnetic relaxation effects. *J Am Chem Soc* 128(41): 13474–13478
- Chang CE, Chen CY, Chen HY (1999) Determination of stability constants of metal complexes by capillary electrophoresis. *J Chin Chem Soc* 46(4):519–528
- Dose A, Liokatis S, Theillet FX, Selenko P, Schwarzer D (2011) NMR profiling of histone deacetylase and acetyl-transferase activities in real time. *ACS Chem Biol* 6(5):419–424
- Eletsky A, Moreira O, Kovacs H, Pervushin K (2003) A novel strategy for the assignment of side-chain resonances in completely deuterated large proteins using C-13 spectroscopy. *J Biomol NMR* 26(2):167–179
- Emsley L, Bodenhausen G (1992) Optimization of shaped selective pulses for Nmr using a quaternion description of their overall propagators. *J Magn Reson* 97(1):135–148
- Farjon J, Boisbouvier J, Schanda P, Pardi A, Simorre JP, Brutscher B (2009) Longitudinal-relaxation-enhanced NMR experiments for the study of nucleic acids in solution. *J Am Chem Soc* 131(24): 8571–8577
- Felli IC, Brutscher B (2009) Recent advances in solution NMR: fast methods and heteronuclear direct detection. *Chemphyschem* 10(9–10):1356–1368
- Hiller S, Wider G, Etezady-Esfarjani T, Horst R, Wuthrich K (2005) Managing the solvent water polarization to obtain improved NMR spectra of large molecular structures. *J Biomol NMR* 32(1):61–70
- Hoyer W, Antony T, Cherny D, Heim G, Jovin TM, Subramaniam V (2002) Dependence of alpha-synuclein aggregate morphology on solution conditions. *J Mol Biol* 322(2):383–393
- Ito Y, Selenko P (2010) Cellular structural biology. *Curr Opin Struct Biol* 20(5):640–648
- Linsler R, Chevelkov V, Diehl A, Reif B (2007) Sensitivity enhancement using paramagnetic relaxation in MAS solid-state NMR of perdeuterated proteins. *J Magn Res* 189(2):209–216
- Liokatis S, Dose A, Schwarzer D, Selenko P (2010) Simultaneous detection of protein phosphorylation and acetylation by high-resolution NMR spectroscopy. *J Am Chem Soc* 132(42): 14704–14705
- Nadaud PS, Helmus JJ, Kall SL, Jaroniec CP (2009) Paramagnetic ions enable tuning of nuclear relaxation rates and provide long-

- range structural restraints in solid-state NMR of proteins. *J Am Chem Soc* 131(23):8108–8120
- Otting G, Liepinsh E (1995) Selective excitation of the water signal by a Q-switched selective pulse. *J Magn Reson B* 107(2):192–196
- Rasia RM, Bertoncini CW, Marsh D, Hoyer W, Cherny D, Zweckstetter M, Griesinger C, Jovin TM, Fernandez CO (2005) Structural characterization of copper(II) binding to alpha-synuclein: insights into the bioinorganic chemistry of Parkinson's disease. *Proc Natl Acad Sci USA* 102(12):4294–4299
- Schanda P (2009) Fast-pulsing longitudinal relaxation optimized techniques: enriching the toolbox of fast biomolecular NMR spectroscopy. *Prog Nucl Magn Reson Spectrosc* 55(3):238–265
- Schanda P, Kupce E, Brutscher B (2005) SOFAST-HMQC experiments for recording two-dimensional heteronuclear correlation spectra of proteins within a few seconds. *J Biomol NMR* 33(4):199–211
- Shaka AJ, Keeler J, Frenkiel T, Freeman R (1983) An improved sequence for broad-band decoupling—waltz-16. *J Magn Reson* 52(2):335–338
- Takeuchi K, Frueh DP, Hyberts SG, Sun ZYJ, Wagner G (2010a) High-resolution 3D CANCA NMR experiments for complete mainchain assignments using C-alpha direct detection. *J Am Chem Soc* 132(9):2945–2951
- Takeuchi K, Frueh DP, Sun ZY, Hiller S, Wagner G (2010b) CACA-TOCSY with alternate  $^{13}\text{C}$ - $^{12}\text{C}$  labeling: a  $^{13}\text{C}$ alpha direct detection experiment for mainchain resonance assignment, dihedral angle information, and amino acid type identification. *J Biomol NMR* 47(1):55–63
- Takeuchi K, Heffron G, Sun ZY, Frueh DP, Wagner G (2010c) Nitrogen-detected CAN and CON experiments as alternative experiments for main chain NMR resonance assignments. *J Biomol NMR* 47(4):271–282
- Uversky VN, Oldfield CJ, Dunker AK (2008) Intrinsically disordered proteins in human diseases: introducing the D2 concept. *Annu Rev Biophys* 37:215–246
- Wickramasinghe NP, Parthasarathy S, Jones CR, Bhardwaj C, Long F, Kotecha M, Mehboob S, Fung LWM, Past J, Samoson A, Ishii Y (2009) Nanomole-scale protein solid-state NMR by breaking intrinsic H-1 T-1 boundaries. *Nat Methods* 6(3):215–218
- Yamamoto K, Xu JD, Kawulka KE, Vederas JC, Ramamoorthy A (2010) Use of a copper-chelated lipid speeds up NMR measurements from membrane proteins. *J Am Chem Soc* 132(20):6929–6931